The Role of Ellis-Van Creveld 2(*EVC2*) in Mice During Cranial Bone Development

EDWIN K. KWON,[1,2] KE'ALE LOUIE,[1] ANSHUL KULKARNI,[1] MARILIA YATABE,[2]
ANTONIO CARLOS DE OLIVEIRA RUELLAS,[2] TAYLOR N. SNIDER,[1,2]
YOSHIYUKI MOCHIDA,[3] LUCIA H. S. CEVIDANES,[2] YUJI MISHINA ,[1†]
AND HONGHAO ZHANG [1†*]

[1]Department of Biologic and Materials Sciences, School of Dentistry, University of
Michigan, Michigan
[2]Department of Orthodontics and Pediatric Dentistry, School of Dentistry, University of
Michigan, Michigan
[3]Department of Molecular and Cell Biology, Henry M. Goldman School of Dental Medicine,
Boston University, Boston, Massachusetts

ABSTRACT

EvC syndrome is a type of autosomal-recessive chondrodysplasia. Previous case studies in patients suggest abnormal craniofacial development, in addition to dwarfism and tooth abnormalities. To investigate how craniofacial development is affected in EvC patients, surface models were generated from micro-CT scans of control mice, *Evc2* global mutant mice and *Evc2* neural crest-specific mutant mice. The anatomic landmarks were placed on the surface model to assess the morphological abnormalities in the *Evc2* mutants. Through analyzing the linear and angular measurements between landmarks, we identified a smaller overall skull, shorter nasal bone, shorter frontal bone, and shorter cranial base in the *Evc2* global mutants. By comparing neural crest-specific *Evc2* mutants with control mice, we demonstrated that the abnormalities within the mid-facial regions are not accounted for by the *Evc2* mutation within these regions. Additionally, we also identified disproportionate length to width ratios in the *Evc2* mutants at all levels from anterior to posterior of the skull. Overall, this study demonstrates a more comprehensive analysis on the craniofacial morphological abnormalities in EvC syndrome and provides the developmental insight to appreciate the impact of *Evc2* mutation within the neural crest cells on multiple aspects of skull deformities. Anat Rec, 301:46–55, 2018. © 2017 Wiley Periodicals, Inc.

Key words: EVC2; LIMBIN; craniofacial development; skull morphology

Ellis-van Creveld syndrome (EvC) is an autosomal-recessive chondrodysplasia (McKusick et al., 1964), with a wide spectrum of symptoms such as shorter limbs and ribs, hypomorphic nails and teeth, polydactyly, and cardiovascular malformations (Baujat and Le Merrer, 2007). Studies have identified *EVC* and *EVC2* as causative genes, which are responsible for around two thirds of identified cases of EvC syndrome in humans (Ruiz-Perez et al., 2000; Ruiz-Perez et al., 2003). Genetic studies have also identified *EVC2/LIMBIN* mutations in Japanese brown cattle (Takeda et al., 2002) and Tyrolean Grey cattle (Murgiano et al., 2014). In both cases,

the affected cattle bear congenital dwarfism, suggesting a conserved function of *EVC2/LIMBIN* during development among different species.

EvC syndrome has been categorized as a ciliopathy due to the ciliary localization of the proteins encoded by *EVC* and *EVC2* (Baujat and Le Merrer, 2007). Recently, *WDR35* was reported as the potential third causative gene for EvC syndrome (Caparros-Martin et al., 2015), though the cells with *WDR35* mutation have quite distinct characteristics. Biochemical studies indicated that EVC and EVC2 are N-terminal anchored transmembrane proteins, which are mutually required for their ciliary localizations (Dorn et al., 2012; Caparros-Martin et al., 2013). The EVC-EVC2 complex interacts with SMO, the Hedgehog signaling effector protein. This interaction at the base of primary cilium is required for transducing Hedgehog signaling (Dorn et al., 2012).

Despite the reports on the function of EVC and EVC2 at the molecular level and the wide spectrum of clinical presentations in EvC patients, the existing documentations of the craniofacial manifestations of EvC syndrome are quite inconsistent. For example, the enlarged skull, depressed nasal bridge, mandibular prognathism characteristic of skeletal class III growth, and skeletal open bite are reported in several cases of EvC patients (Ellis and van Creveld, 1940; Goor et al., 1965; Susami et al., 1999), while other reports indicated that facial development is normal (Varela and Ramos, 1996; Hanemann et al., 2010). These inconsistencies are possibly due to a large variation in the patients' genetic background and/or the limited information on the craniofacial abnormalities in EvC patients.

Previous reports have documented studies using mouse models to understand the pathophysiological mechanism leading to congenital abnormalities in EvC patients. For example, *Evc2* mutant mice bear shortened limbs and abnormally developed teeth, which are similar to symptoms observed in EvC patients (Zhang et al., 2015, 2017). *Evc* or *Evc2* mutant mice were also used as models for understanding the craniofacial abnormalities. However, these works are either restricted to the cranial base at embryonic stages (Pacheco et al., 2012) or mainly focus on the skull deformities in the anterior-posterior dimension (Badri et al., 2016b). Interestingly, it is not known if the mid-facial defect identified in *Evc2* mutant is due to the loss of *Evc2* function within the mid facial region. In this study, to better understand the skull deformities in EvC patients, we use micro-CT based skull modeling to generate three-dimensional surfaces models for the *Evc2* mutant mice. Additionally we also compared the global mutant mice for *Evc2* with the neural crest-specific mutants for *Evc2* to understand the impact of the *Evc2* mutation within the neural crest cells on multiple aspects of the skull deformities.

METHODS AND MATERIALS
Animal Model

Animals were maintained and used in compliance with the Institutional Animal Care and Use Committee (IACUC) of the University of Michigan in accordance with the National Institutes of Health Guidelines for Care and Use of Animals in research and all experimental procedures were approved by the IACUC of the University of Michigan. *Evc2* global and conditional mutant mice used in the current studies were generated by our group and reported previously (Zhang et al., 2015). Global mutant mice (hereafter *Evc2 m*) were obtained by crossing heterozygous male and female mice. Neural crest-specific *Evc2* (hereafter *Evc2 cko*) mutant mice were generated by crossing *Evc2* floxed mice (Zhang et al., 2015) and neural crest specific *Cre* mice (*P0*-Cre, *C57BL/6J-Tg(P0-Cre)94Imeg* (ID 148), provided by Dr. Kenichi Yamamura) (Yamauchi et al., 1999). *Evc2* global mutant and floxed mice were maintained in a mixed background of C57BL6/J and 129S6. All mice were crossed and maintained in our semi-closed mouse colony for at least 5 years.

Histological Analysis

Heads from mice with different genotypes at postnatal day 8 were collected and fixed in 4% Paraformaldehyde overnight. They were then preserved in phosphate buffered saline (PBS) until micro-CT scanning was obtained on all skulls.

Micro-CT (μCT)

Micro-CT scanning of fixed skulls was taken at the University of Michigan using a micro-CT system (μCT100 Scanco Medical, Bassersdorf, Switzerland). Scan settings were as following: voxel size 12 μm, 55 kVp, 109 μA, 0.5 mm AL filter, and integration time 500 ms.

Image Acquisition, Segmentation, and Surface Models

To quantify the skull morphological differences among controls, *Evc2 m* and *Evc2 cko* at postnatal day 8, the surface models were first generated based on micro-CT data, as shown in Figure 1. Digital Image and Communications in Medicine (DICOM) files/images obtained from micro-CT were used to generate 3D model using ITK-SNAP (open-source software developed by grants and contracts from the US National Institutes of Health, www.itksnap.org). The 3D slicer (open-source software, www.slicer.org) was then used for placements of anatomical landmarks. Model superimpositions were carried out using 3D Slicer with the following landmarks on the occipital bones: right and left anterolateral tips of the interparietal bone, cross point between the median line and the line which connects left and right anterolateral tip of the interparietal bone, and posterior tip of the interparietal bone.

Landmark Identification

Overall, fifteen surface models were generated and 19 landmarks (Table 1) were placed on each sample for linear measurements in all three dimensions, for angular measurements (Table 2) and for width to length ratio calculations.

Statistical Analysis

The Mann–Whitney U test was done by SPSS 21.0 to evaluate the linear and angular measurements between controls and mutants.
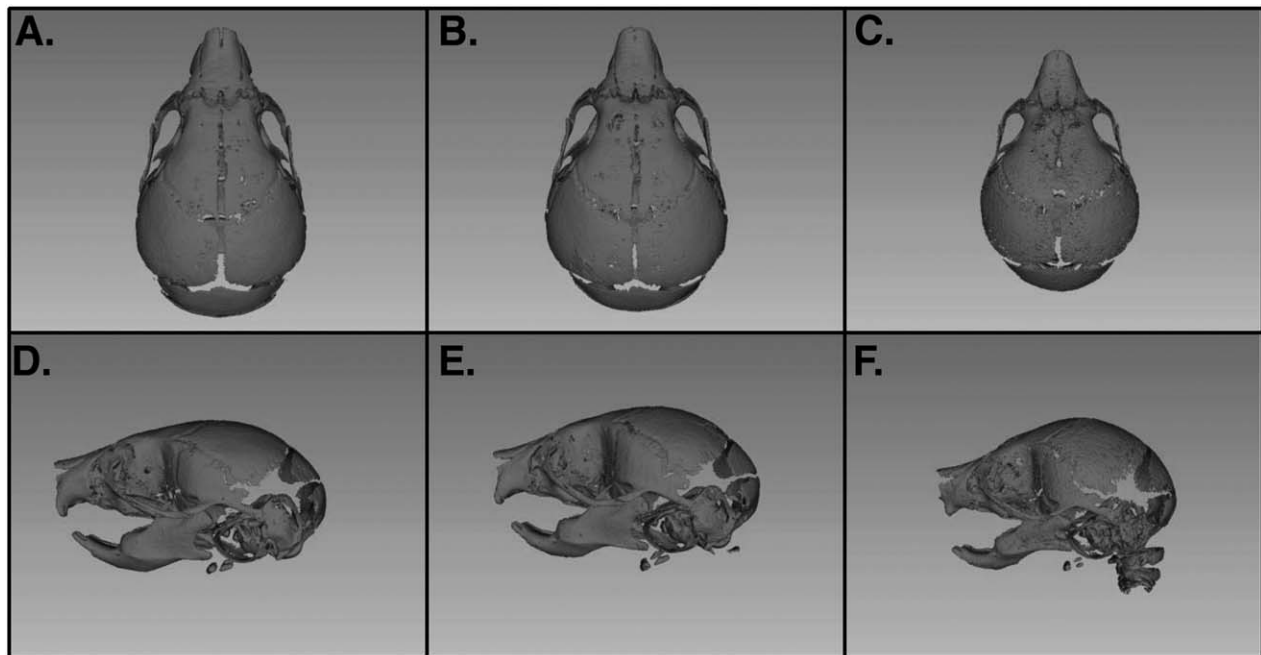
Fig. 1. Gross morphology of head in control, *Evc2 cko* and *Evc2 m*. Dorsal views (A–C) and left lateral views (D–F) of represented control, *Evc2 cko*, and *Evc2 m*, respectively.

TABLE 1. Craniofacial landmarks

Anatomical landmarks	Description
A	Nasale, Rostral point of nasal bone
N	Nasion, Caudal point of nasal bone
F	Caudal point of frontal bone
Pr	Caudal point of Parietal bone
Pri	Most posterior point of interparietal bone at midline
XN	Most anterior point at intersection of premaxillae and nasal bones
XMx	Most inferior point of premaxilla at Premaxilla-maxilla suture
ZMx	Most anterior point of zygomatic process of zygoma at intersection of maxilla and zygoma
MxSp	Most posterior point of alveolar ridge at the Intersection of maxilla and sphenoid
ZT	Most anterior point of Zygomatic process of temporal bone at intersection of zygoma and zygomatic process of temporal bone
Tp	Most posterior portion of post-tympanic hook of temporal bone
PNS	Posterior nasal spine
Pf	Posterior palatine fissure
Sp	Intersection of presphenoid and frontal bone at midline of cranial base
Sos	At SOS, sphenoid-occipital suture, most anterosuperior point
Ba	Basion
Op	Opisthion
MxAl	Most inferior point at center of alveolar ridge on the lingual side of maxillary incisor, lingual
MxC	Maxillary incisor edge

Please note that bilateral anatomical points are labeled left side first. Anatomical landmarks in parentheses are midpoints of the bilateral landmarks.

RESULTS

Generated *Evc2 m* and *Evc2 cko* (Zhang et al., 2015) had a gross morphology similar to those seen in EvC patients as well as in the *Evc* mutant mice (McKusick et al., 1964; Ruiz-Perez et al., 2007). In comparison to controls, both types of mutants showed shortened skull length, while the length of the skull is more severely affected in *Evc2 m* compared to *Evc2 cko* (Fig. 1).

For cranial base length I (Sp-Sos), erupted upper incisor length (MxAl-MxC), and total Cranial Base (A-Ba), we observed significant differences when comparing *Evc2 m* to control and comparing *Evc2 cko* to control (Table 3, Figs. 2B–D and 3B). These results suggest that *Evc2* function in the neural crest cells affects the development of these regions. In contrast, we observed no differences in the width of the nasal bone at the

TABLE 2. Linear and angular measurements

Linear measurements	Anatomical landmarks	Angular measurements	Anatomical landmarks
Total skull length	A-Pri	Neurocranium to Cranial Base I	A-N/A-Ba
Nasomaxillary complex		Neurocranium to Cranial Base II	N-F/A-Ba
Nasal bone length	A-N	Cranial base to Vault I	N-F/F-Pr
Frontal bone length	N-F	Cranial base to Vault II	F-Pr/Pr-Pri
Width of nasal bone at intersection with premaxillae	Xn-Xn	Cranial vault to cranial base I	F-Pri/F-Ba
Zygomatic arch length	ZMx-ZT	Cranial vault to cranial base II	F-Pri/Sp-SOS
Erupted upper incisor length	MxAl-MxC	Cranial vault to cranial base III	F-Pri/Sp-Ba
Viscerocranial length	F-MxAl	Cranial vault to cranial base IV	F-Pri/Sos-Ba
Calvaria		Nasal bone to cranial base I	A-N/F-Ba
Parietal length	F-Pr	Nasal bone to cranial base II	A-N/Sp-Sos
Interparietal length	Pr-Pri	Nasal bone to cranial base III	A-N/Sp-Ba
Occipital Bone	Pri-Op	Nasal bone to cranial base IV	A-N/Sos-Ba
Width at Zygomatic arch (anterior)	ZMx-ZMx	Nasal bone to cranial vault	A-N/F-MxAl
Width at Zygomatic arch (posterior)	ZT-ZT	Premaxilla to cranial base	F-MxAl/F-Ba
Width of temporal bone	Tp-Tp	Upper incisors to cranial base	F-MxC/F-Ba
Cranial Base		Premaxilla to cranial vault	F-MxAl/F-Pri
Total Cranial Base	A-Ba	Upper incisors to cranial vault	F-MxC/F-MxAl
Cranial base length I	Sp-Sos		
Cranial base length II	Sp-Ba		
Basioccipital length	Ba-Sos		
Viscerocranial heights			
Viscerocranial height at SOS	F-Sos		
Viscerocranial height at basion	F-Ba		

TABLE 3. 1: Control group, 2: *Evc2 P0m*, 3: *Evc2m*

Measurements	Group vs. Group	Change mm	Change %	P value	Measurements	Group vs. Group	Change mm	Change %	P value
A-Pri	1–2	0.534	3.523	#	ZT-ZT	1–2	0.047	0.532	#
	1–3	1.623	10.715	***		1–3	0.702	7.985	***
	2–3	1.089	7.454	**		2–3	0.656	7.493	***
A-N	1–2	0.204	5.163	#	Tp-Tp	1–2	−0.099	−1.077	#
	1–3	0.484	12.262	***		1–3	0.684	7.439	***
	2–3	0.280	7.486	*		2–3	0.783	8.426	***
N-F	1–2	0.072	1.207	#	A-Ba	1–2	0.787	5.870	**
	1–3	0.636	10.725	**		1–3	1.902	14.196	***
	2–3	0.564	9.634	**		2–3	1.116	8.845	***
XN-XN	1–2	−0.005	−0.217	#	Sp-Sos	1–2	1.509	28.731	#
	1–3	0.034	1.487	#		1–3	2.677	50.984	*
	2–3	0.039	1.701	#		2–3	1.169	31.224	#
ZMx-ZT	1–2	0.148	5.118	#	Sp-Ba	1–2	1.097	14.658	#
	1–3	0.448	15.479	**		1–3	2.083	27.839	**
	2–3	0.300	10.920	***		2–3	0.986	15.444	#
MxAl-MxC	1–2	0.122	19.295	**	Sos-Ba	1–2	−0.040	−1.535	#
	1–3	0.374	59.378	***		1–3	−0.210	−8.004	***
	2–3	0.253	49.666	***		2–3	−0.169	−6.371	**
F-MxAl	1–2	0.132	1.312	#	F-Sos	1–2	0.113	1.759	#
	1–3	1.052	10.495	**		1–3	0.288	4.487	*
	2–3	0.921	9.305	*		2–3	0.175	2.777	#
F-Pr	1–2	0.055	1.567	#	F-Ba	1–2	0.103	1.298	#
	1–3	0.370	10.530	#		1–3	0.022	0.283	#
	2–3	0.315	9.106	#		2–3	−0.080	−1.029	#
Pr-Pri	1–2	−0.021	−0.685	#					
	1–3	−0.624	−19.990	***					
	2–3	−0.603	−19.173	***					
Pri-Op	1–2	0.059	2.678	#					
	1–3	0.330	14.946	***					
	2–3	0.271	12.606	***					
ZMx-ZMx	1–2	−0.064	−0.852	#					
	1–3	0.616	8.177	***					
	2–3	0.681	8.953	***					

Changes in linear measurements are indicated as mm and percentage. Positive value indicates decrease in the latter sample comparing to former sample. Negative values indicate an increase in the latter sample comparing to former sample. $N = 5$, #, $P > 0.05$; *, $P < 0.05$; **, $P < 0.01$; ***, $P < 0.001$.

A.

B. **Total skull (A-Pri)**

C. **Nasal bone (A-N)**

D. **Frontal bone (N-F)**
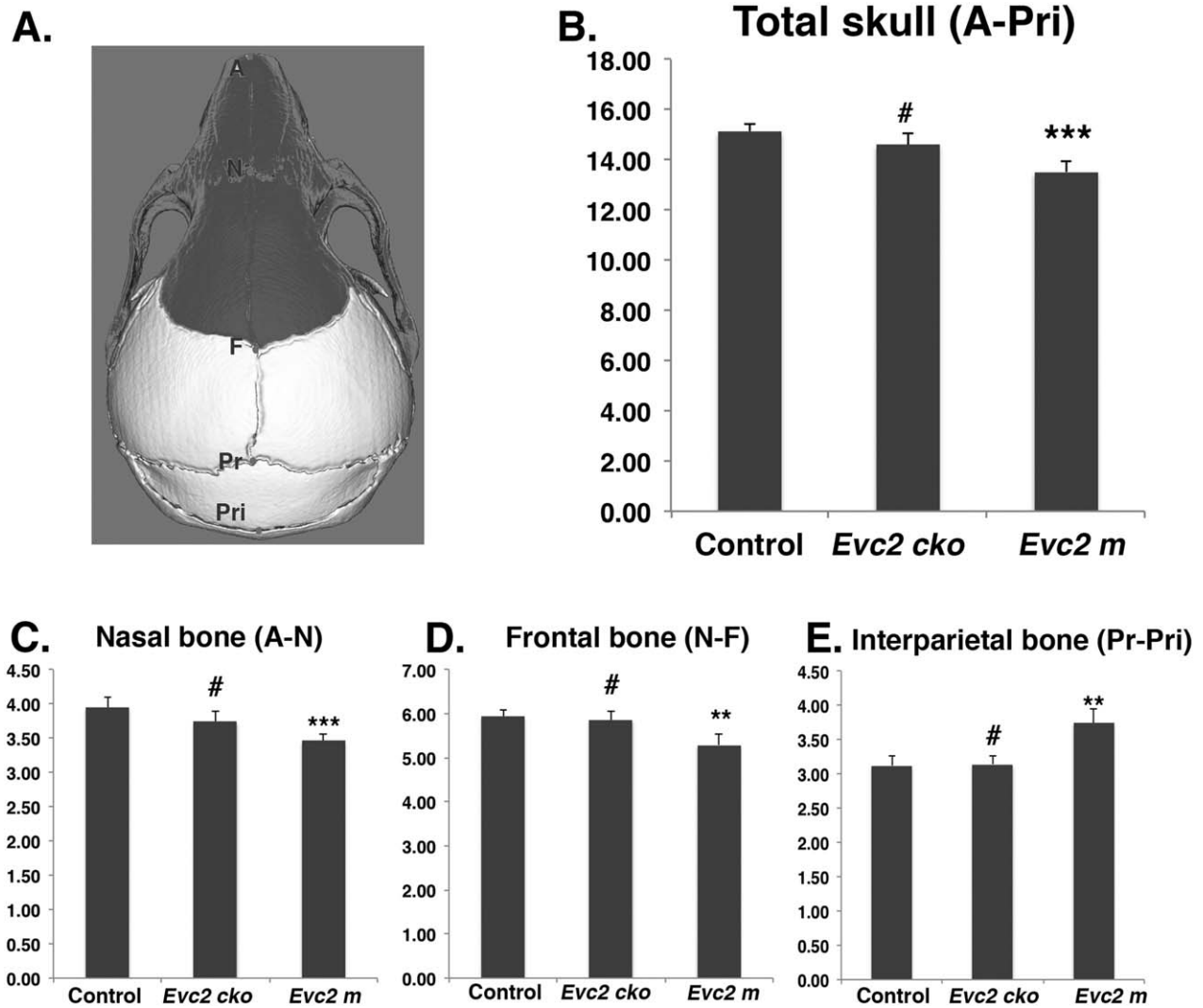

E. **Interparietal bone (Pr-Pri)**

Fig. 2. *Evc2* mutation leads to abnormal head in anterior posterior dimension. A. Diagram indicates the landmarks in the anterior posterior dimension. Areas with dark color are derived from neural crest cells. The length of total (B), nasal bone (C), frontal bone (D) and interparietal bone (E) are shown. $N = 5$, #, $P > 0.05$; *, $P < 0.05$; **, $P < 0.01$; ***, $P < 0.001$.

intersection with premaxillae (Xn-Xn), parietal length (F-Pr), or viscerocranial height at basion (F-Ba) (Table 3), suggesting that these characteristics are not affected by *Evc2* mutations. For skull length (A-Pri), nasal bone length (A-N), frontal bone length (N-F), zygomatic arch length (ZMx-ZT), viscerocranial length (F-MxAl), interparietal length (Pr-Pri), occipital bone length (Pri-Op), width of anterior zygomatic arch (ZMx-ZMx), width of posterior zygomatic arch (ZT-ZT), width of temporal bone (TP-TP), basioccipital length (Sos-Ba), cranial base length II (Sp-Ba), and viscerocranial height at Sos (F-Sos), we only detected significant differences between control and *Evc2 m*, but not between control and *Evc2 cko* (Figs. 2B–E and. 3E, and Table 3), suggesting that *Evc2* function in non-neural crest derived tissues may play a vital role in the development of these tissues. Overall, comparisons of the linear measurements between controls, *Evc2 m*, and *Evc2 cko* allow the identification of the origins of the tissues leading to the linear

abnormalities during skull development. To examine if the shortened cranial base observed in the *Evc2 m* and *Evc2 cko* is due to early synchondrosis fusion, we generated the models including the cranial bases from the CT scans (Fig. 3F–H). The CT scans clearly indicate early fusion of the intersphenoidal synchondrosis in the *Evc2 m*, but not in the controls or in *Evc2 cko*.

Based on angular measurements comparing control with *Evc2 m* and control with *Evc2 cko*, we observed no differences (Table 4) in cranial vault to cranial base III (F-Pri/Sp-Ba) or cranial vault to cranial base IV (F-Pri/ Sos-Ba), suggesting that these characteristics are not affected by *Evc2* mutations. For neurocranium to cranial base II (A-F/A-Ba), Cranial base to Vault I (N-F/F-Br), nasal bone to cranial base I (A-N/F-Ba), premaxilla to cranial base (MxAl-F/F-Ba), upper incisors to cranial base (MxC-F/F-Ba), premaxilla to cranial vault (MxAl-F/ Sp-Ba), and upper incisors to cranial vault (MxC-F/ F-MxAl), we observed significant differences when
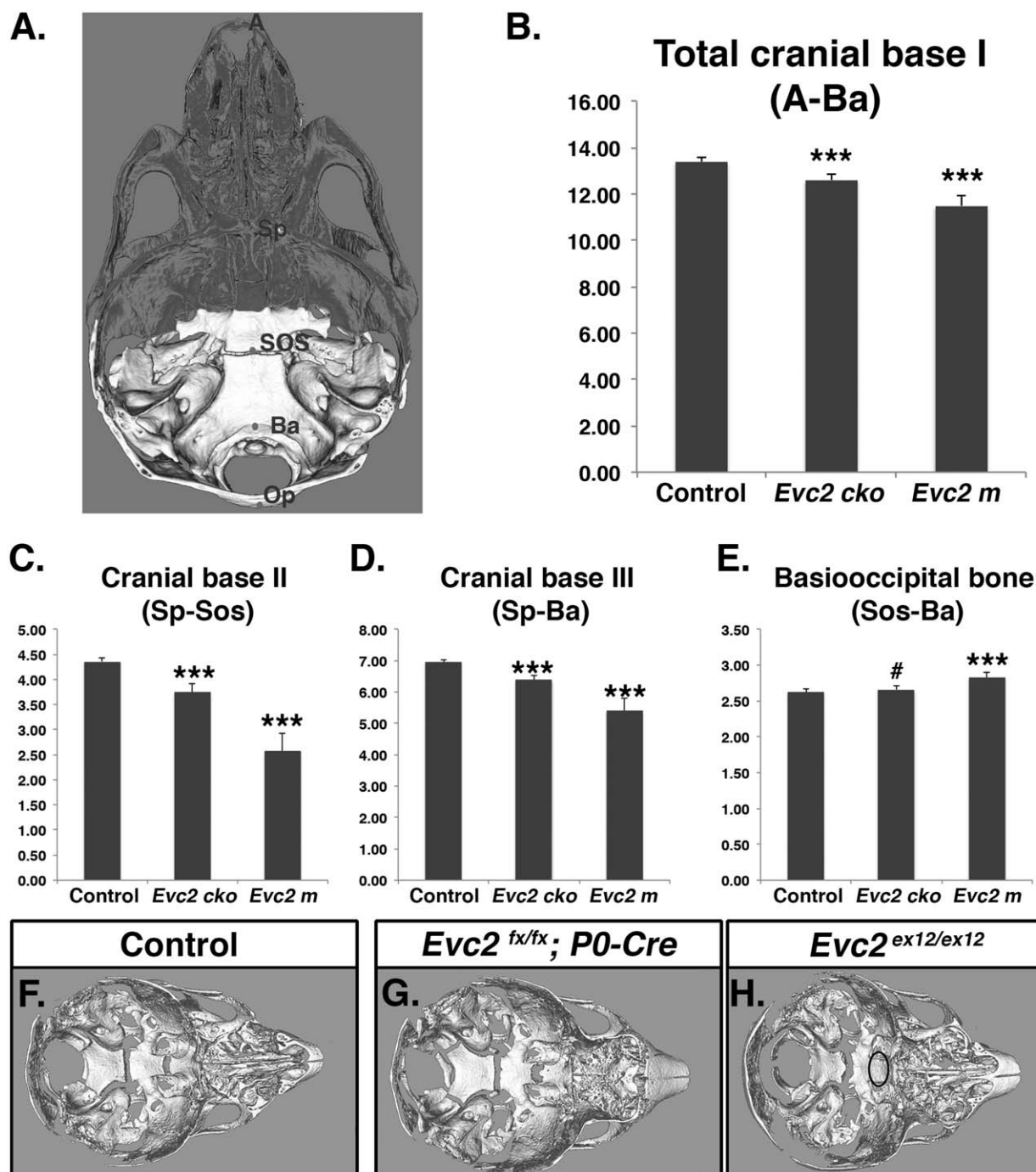
Fig. 3. *Evc2* mutation leads to abnormal cranial base. A. Diagram indicates the landmarks in the cranial base. Areas with dark color are derived from neural crest cells. The lengths of the cranial base at different levels are shown in (B–E). $N = 5$, #, $P > 0.05$; ***, $P < 0.001$. F–H. Cranial base models generated from the μCT scans of control (F), *Evc2 cko* (G) and *Evc2 m* (H). Dark circle indicates the fused ISS in *Evc2 m*.

comparing *Evc2 m* to control and comparing *Evc2 cko* to control, suggesting that *Evc2* function in the neural crest-derived cells plays a vital role for the development of these tissues. For neurocranium to cranial base I (A-N/A-Ba), cranial base to Vault II (F-Pr/Pr-Pri), cranial vault to cranial base I (F-Pri/F-Ba), nasal bone to cranial base IV (A-N/Sp-Ba), and nasal bone to cranial vault (A-N/F-MxAl), we only detected significant differences (Table 4) between control and *Evc2 m*, but not between control and *Evc2 cko*. Overall, comparisons of the angular measurements between controls, *Evc2 m*, and *Evc2 cko* allow for the identification of the origins of the tissues leading to the angular abnormalities during skull development.

TABLE 4. 1: Control group, 2: *Evc2 P0m*, 3: *Evc2m*

Measurements	Group vs Group	Change in degree	p value	Measurements	Group vs Group	Change in degree	p value
A-N/A-Ba	1–2	−1.876	#	A-N/Sp-Ba	1–2	−0.937	#
	1–3	−4.089	**		1–3	−5.997	**
	2–3	−2.214	#		2–3	−5.060	*
A-F/A-Ba	1–2	−2.355	**	A-N/Sos-Ba	1–2	−4.404	#
	1–3	−7.439	***		1–3	−10.925	**
	2–3	−5.084	***		2–3	−6.521	*
N-F/F-Pr	1–2	4.305	**	A-N/F-MxAl	1–2	−0.257	#
	1–3	9.210	***		1–3	−4.306	**
	2–3	4.906	***		2–3	−4.049	**
F-Pr/Pr-Pri	1–2	0.984	#	MxAl-F/F-Ba	1–2	4.665	**
	1–3	6.602	***		1–3	11.063	***
	2–3	5.618	***		2–3	6.398	***
F-Pri/F-Ba	1–2	−0.387	#	MxC-F/F-Ba	1–2	3.633	**
	1–3	2.430	***		1–3	8.990	***
	2–3	2.817	***		2–3	5.356	***
F-Pri/Sp-Ba	1–2	−1.017	#	MxAl-F/F-Pri	1–2	4.288	**
	1–3	−0.971	#		1–3	13.504	***
	2–3	0.046	#		2–3	9.215	***
F-Pri/Sos-Ba	1–2	0.379	#	MxC-F/F-MxAl	1–2	−1.032	**
	1–3	1.736	#		1–3	−2.074	***
	2–3	1.358	#		2–3	−1.042	**
A-N/F-Ba	1–2	−4.408	*				
	1–3	−6.758	***				
	2–3	−2.350	#				

Changes in angular measurements (degree only). Positive value indicates decrease in the latter sample comparing to former sample. Negative values indicate an increase in the latter sample comparing to former sample. $N = 5$, #, $P > 0.05$; *, $P < 0.05$; **, $P < 0.01$; ***, $P < 0.001$.

In addition to the linear and angular measurements, we also accessed the width to length ratios. These ratio calculations were taken by using two individuals in the anterior half of the skull and two individuals in the posterior half of the skull divided by the total skull length. For the ratio at the premaxilla level, we only detected significant differences (Fig. 4B) in the comparison between control and *Evc2 m*, but not in the comparison between control and *Evc2 cko*, suggesting that only *Evc2 m* bears a disproportionately wider skull at this level and *Evc2 cko* does not. For the ratios at the anterior of zygomatic level, posterior of zygomatic level and temporal level, we detected significant differences (Fig. 4C–E) within comparisons of control with *Evc2 m* and control with *Evc2 cko*, suggesting that both *Evc2 m* and *Evc2 cko* bear a disproportionately wider skull at these three levels.

To appreciate the overall skull differences in the anterior–posterior axis between control and *Evc2 m* and *Evc2 cko*, we generated the surface models for each genotype and superimposed the mutant skulls onto the control skulls (Fig. 5). Superimposition was anchored at the posterior end of the skull, because most of the deformities were identified in the anterior region. Consistent with the aforementioned linear and angular measurements, we observed most differences between control skulls and *Evc2 m* skulls in the anterior–posterior axis. Particularly, in the *Evc2 m* skull, an apparent shallow mid-facial region is observed. On the other hand, minimal differences in the mid-facial region are observed when comparing control skulls with *Evc2 cko*.

DISCUSSIONS

Craniofacial abnormalities were previously documented and suggested by different EvC case studies (McKusick et al., 1964; Baujat and Le Merrer, 2007). To get more insight into how craniofacial development is affected in EvC syndrome, we carried out an investigation to understand the morphological abnormalities of EvC syndrome using 3D imaging software on *Evc2* mutant mouse models. We also took advantage of a conditional deletion system to generate neural crest-specific *Evc2* mutants, allowing us to trace the origin of morphological abnormalities during development. Overall, our studies demonstrated a more comprehensive analysis of the craniofacial morphological abnormalities and provided the developmental insight to appreciate the origin of these abnormalities.

EVC and EVC2, the proteins encoded by the two causative genes of EvC syndrome, form a protein complex at the base of primary cilium, which is mutually required for cilium localization and for transducing Hedgehog signaling (Dorn et al., 2012; Caparros-Martin et al., 2013). At postnatal day 8, *Evc2 m* exhibited smaller skull size compared to the control group. The gross morphology demonstrated in the *Evc2* mutant mice is similar both to phenotypes of *Evc* mutant mice (Ruiz-Perez et al., 2007; Pacheco et al., 2012; Badri et al., 2016b) and to symptoms observed in EvC patients (Ellis and van Creveld, 1940; McKusick et al., 1964). These facts suggest that the molecular pathological mechanism leading to craniofacial abnormalities in *Evc2* mutant mice is the same as those in *Evc* mutant mice and in EvC patients.
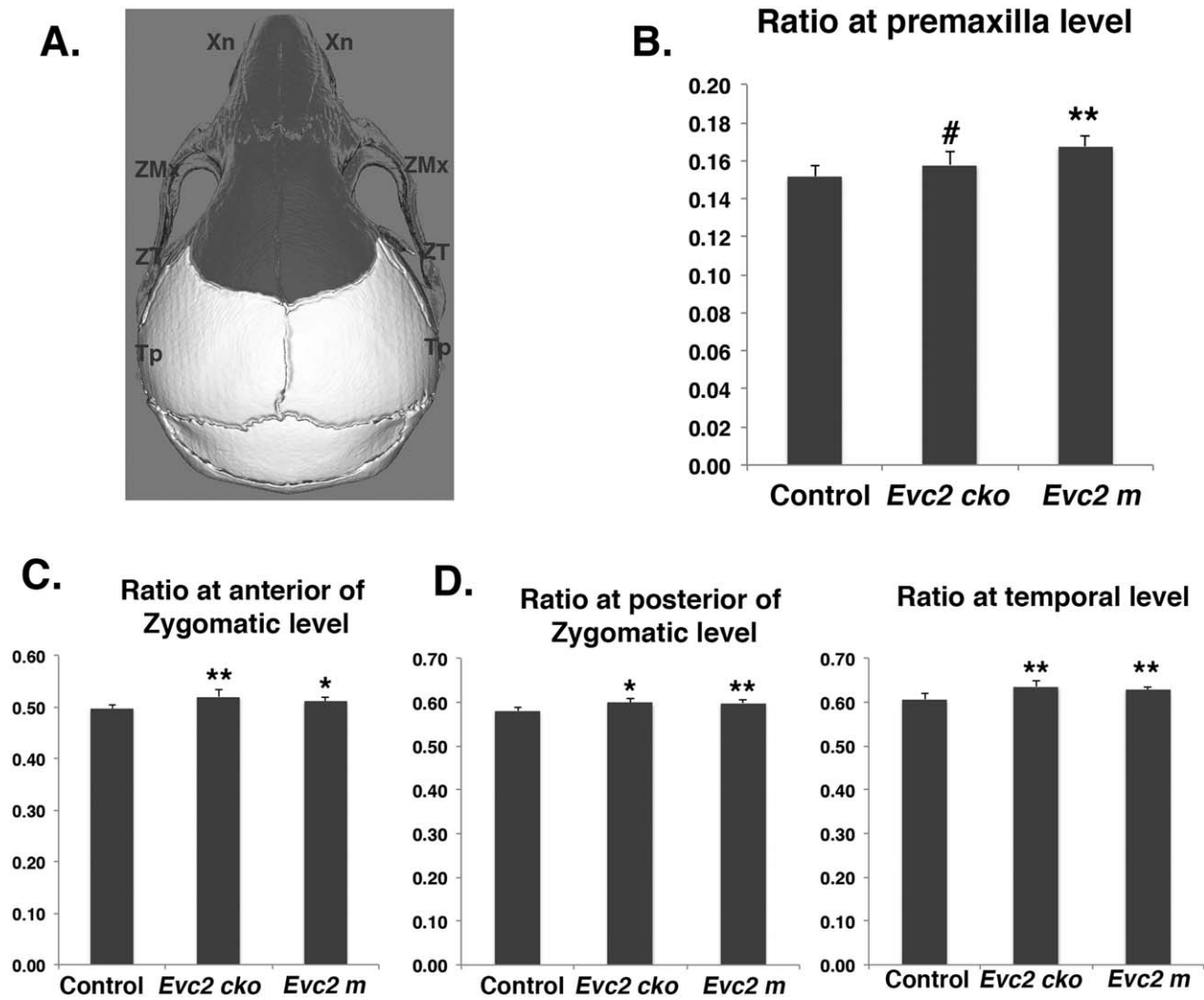
Fig. 4. Width over length ratios of *Evc2* mutant skulls at different levels. A. Diagram indicates the landmarks associated with width measurement. Areas with dark color are derived from neural crest cells. Width over length ratios at Premaxilla level (B), anterior of Zygomatic level (C), posterior of Zygomatic level (D) and temporal level (E) were shown. $N = 5$, #, $P > 0.4$; *, $P < 0.05$; **, $P < 0.01$.

In the current studies, we identified that the skull length, nasal bone length, frontal bone length, incisor length, and total cranial base length are all significantly smaller in *Evc2 m* mutants than in controls at postnatal day 8. These observations are consistent with previous reports using different methods to study abnormal craniofacial development (Badri et al., 2016b) and abnormal tooth development (Zhang et al., 2015, 2017). Our previous studies demonstrated that *Evc2* is expressed in nearly all tissues in the skull (Badri et al., 2016a). Because the nasal and frontal bones are developmentally derived from neural crest cells, the reasonable speculation is that *Evc2* function in the neural crest cells leads to shortened nasal and frontal bones. In contrast, the nasal bone length and frontal bone length in *Evc2 cko* mutants remain the same as in the controls. The efficient Cre recombination within the neural crest cells mediated by *P0*-Cre (data not shown) suggests that *Evc2* function within the nasal and frontal bones does not play a major role in determining the length of these two bones.

In addition to the abnormalities detected in the mid facial region, we also detected a shortened cranial base. Our paired comparisons suggest that cranial base length is more severely affected in *Evc2* global mutants (14.2% decrease) than in *Evc2 cko* (5.9% decrease). The cranial base is a midline structure which connects several bones in the cranial and facial regions (Nie, 2005). It has unique embryologic developmental origins, with the anterior region being derived from the neural crest and the posterior region from the mesoderm (Nie, 2005; McBratney-Owen et al., 2008). Consistently, at P8, we observed early closure of the intersphenoidal synchondrosis in *Evc2* global mutants, but not in the *Evc2 cko*. Previous studies demonstrated that a shortening of the cranial base during development leads to a number of mid-facial abnormalities. For example, the retrognathic facial profile characteristic of Cretinism, Turner
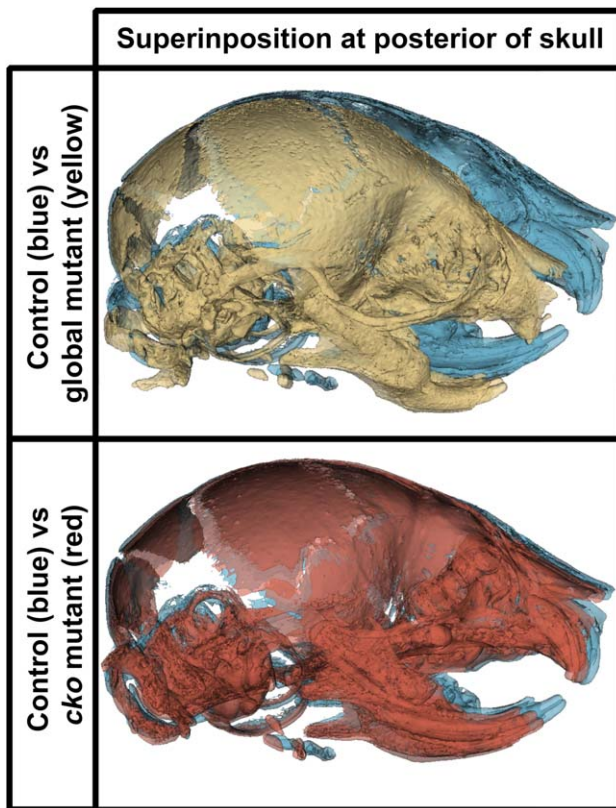
Fig. 5. Superimpositions of skulls between controls and *Evc2 cko* and *Evc2 m*. A. Superimpositions of *Evc2 m* (yellow) with control skull (blue). B. Superimpositions of *Evc2 cko* (red) with control skull (blue).

syndrome, and Down's syndrome is due to reduced cranial base length (Israel et al., 1983; Jensen, 1985; Rongen-Westerlaken et al., 1992; Midtbo et al., 1996; Andersen et al., 2000; Quintanilla et al., 2002). Similar trends are also identified in Klinefelter syndrome and Williams's syndrome (Mass and Belostoky, 1993; Brkic et al., 1994). Given the function of cranial base in mid-facial bone development, it is possible that the severely affected cranial base observed in the *Evc2* global mutant mice leads to the shortened nasal and frontal bones during the early skull development. Currently we are carrying out studies to validate this possibility at different time points during post-natal skull development.

Additionally, we also observed that the widths at the zygomatic arch (both anterior and posterior regions) and the width at the temporal bone level are all significantly smaller compared to controls, while there are no differences in the width of the nasal bone at the premaxilla level. On the other hand, the decreased width is less likely due to the decreased size of the overall skull, because the ratios of the width to the skull length are all significantly increased in *Evc2 m* and *Evc2 cko* mutant mice.

Compared to controls, the skull from *Evc2 m* mutants showed increased interparietal length (Pr-Pri) and increased basioccipital length (Sos-Ba) (Fig. 3E), in contrast with decreased nasal bone length and frontal bone length. It is possible that these length increases are to compensate the decreased skull volume in the anterior

region. However, in the *Evc2 cko* mutant, where we observed a similar mid-facial defect and decreased skull volume in the anterior head as in *Evc2 m*, we could not detect any increased interparietal length (Pr-Pri) and increased basioccipital length (Sos-Ba). It is possible that loss of *Evc2* function in the non-neural crest-derived tissue promotes the over growth of these bones. Further genetic experiments to specifically delete *Evc2* in the mesoderm-derived tissues are needed.

In conclusion, our study presents a comprehensive characterization of altered craniofacial development in the *Evc2* mutant mice, and provides the developmental insight to appreciate the origin of each morphological abnormality.

ACKNOWLEDGEMENTS

LITERATURE CITED

Andersen E, Sonnesen L, Kjaer MS, Fischer Hansen B, Kjaer I. 2000. The prenatal cranial base complex and hand in Turner syndrome. Eur J Orthodont 22:185–194.

Badri MK, Zhang H, Ohyama Y, Venkitapathi S, Alamoudi A, Kamiya N, Takeda H, Ray M, Scott G, Tsuji T, et al. 2016a. Expression of Evc2 in craniofacial tissues and craniofacial bone defects in Evc2 knockout mouse. Arch Oral Biol 68:142–152.

Badri MK, Zhang H, Ohyama Y, Venkitapathi S, Kamiya N, Takeda H, Ray M, Scott G, Tsuji T, Kunieda T, Mishina Y, Mochida Y. 2016b. Ellis van Creveld2 is required for postnatal craniofacial bone development. Anat Rec 299:1110–1120.

Baujat G, Le Merrer M. 2007. Ellis-van Creveld syndrome. Orphanet J Rare Dis 2:27.

Brkic H, Kaic Z, Poje Z, Singer Z. 1994. Shape of the craniofacial complex in patients with Klinefelter syndrome. Angle Orthod 64: 371–376.

Caparros-Martin JA, Valencia M, Reytor E, Pacheco M, Fernandez M, Perez-Aytes A, Gean E, Lapunzina P, Peters H, Goodship JA, et al. 2013. The ciliary Evc/Evc2 complex interacts with Smo and controls Hedgehog pathway activity in chondrocytes by regulating Sufu/Gli3 dissociation and Gli3 trafficking in primary cilia. Hum Mol Genet 22:124–139.

Caparros-Martin JA, De Luca A, Cartault F, Aglan M, Temtamy S, Otaify GA, Mehrez M, Valencia M, Vazquez L, Alessandri JL, et al. 2015. Specific variants in WDR35 cause a distinctive form of Ellis-van Creveld syndrome by disrupting the recruitment of the EvC complex and SMO into the cilium. Hum Mol Genet 24:4126–4137.

Dorn KV, Hughes CE, Rohatgi R. 2012. A smoothened-Evc2 complex transduces the Hedgehog signal at primary cilia. Dev Cell 23: 823–835.

Ellis RW, van Creveld S. 1940. A syndrome characterized by ectodermal dysplasia, polydactyly, chondro-dysplasia and congenital morbus cordis: Report of three cases. Arch Dis Child 15:65–84.

Goor D, Rotem Y, Friedman A, Neufeld HN. 1965. Ellis-Van Creveld syndrome in identical twins. Br Heart J 27:797.

Hanemann JA, de Carvalho BC, Franco EC. 2010. Oral manifestations in Ellis-van Creveld syndrome: report of a case and review of the literature. J Oral Maxillofac Surg 68:456–460.

Israel H, Johnson GF, Fierrobenitez R. 1983. Craniofacial Malformation among Endemic Cretins in Ecuador. J Cran Genet Dev Bio 3:3–10.

Jensen BL. 1985. Craniofacial morphology in Turner syndrome. J Craniofac Genet Dev Biol 5:327–340.

Mass E, Belostoky L. 1993. Craniofacial morphology of children with Williams syndrome. Cleft Palate-Cran J 30:343–349.

McBratney-Owen B, Iseki S, Bamforth SD, Olsen BR, Morriss-Kay GM. 2008. Development and tissue origins of the mammalian cranial base. Dev Biol 322:121–132.

McKusick VA, Egeland JA, Eldridge R, Krusen DE. 1964. Dwarfism in the Amish I. The Ellis-Van Creveld Syndrome. Bull Johns Hopkins Hosp 115:306–336.

Midtbo M, Wisth PJ, Halse A. 1996. Craniofacial morphology in young patients with Turner syndrome. Eur J Orthodont 18:215–225.

Murgiano L, Jagannathan V, Benazzi C, Bolcato M, Brunetti B, Muscatello LV, Dittmer K, Piffer C, Gentile A, Drogemuller C. 2014. Deletion in the EVC2 gene causes chondrodysplastic dwarfism in Tyrolean Grey cattle. PLoS One 9:e94861.

Nie X. 2005. Cranial base in craniofacial development: Developmental features, influence on facial growth, anomaly, and molecular basis. Acta Odontol Scand 63:127–135.

Pacheco M, Valencia M, Caparros-Martin JA, Mulero F, Goodship JA, Ruiz-Perez VL. 2012. Evc works in chondrocytes and osteoblasts to regulate multiple aspects of growth plate development in the appendicular skeleton and cranial base. Bone 50:28–41.

Quintanilla JS, Biedma BM, Rodirguez MQ, Mora MTS, Cunqueiro MMS, Pazos MA. 2002. Cephalometrics in children with Down's syndrome. Pediatr Radiol 32:635–643.

Rongen-Westerlaken C, vd Born E, Prahl-Andersen B, Rikken B, Teunenbroek V, Kamminga N, vd Tweel I, Otten BJ, Delamarre vd Waal HA, Drayer NM, et al. 1992. Shape of the craniofacial complex in children with Turner syndrome. J Biol Buccale 20:185–190.

Ruiz-Perez VL, Ide SE, Strom TM, Lorenz B, Wilson D, Woods K, King L, Francomano C, Freisinger P, Spranger S, et al. 2000. Mutations in a new gene in Ellis-van Creveld syndrome and Weyers acrodental dysostosis. Nat Genet 24:283–286.

Ruiz-Perez VL, Tompson SW, Blair HJ, Espinoza-Valdez C, Lapunzina P, Silva EO, Hamel B, Gibbs JL, Young ID, Wright MJ, et al. 2003. Mutations in two nonhomologous genes in a head-to-head configuration cause Ellis-van Creveld syndrome. Am J Hum Genet 72:728–732.

Ruiz-Perez VL, Blair HJ, Rodriguez-Andres ME, Blanco MJ, Wilson A, Liu YN, Miles C, Peters H, Goodship JA. 2007. EVC is a positive mediator of IHH-regulated bone growth that localises at the base of chondrocyte cilia. Development 134:2903–2912.

Susami T, Kuroda T, Yoshimasu H, Suzuki R. 1999. Ellis-van Creveld syndrome: Craniofacial morphology and multidisciplinary treatment. Cleft Palate-Cran J 36:345–352.

Takeda H, Takami M, Oguni T, Tsuji T, Yoneda K, Sato H, Ihara N, Itoh T, Kata SR, Mishina Y, et al. 2002. Positional cloning of the gene LIMBIN responsible for bovine chondrodysplastic dwarfism. Proc Natl Acad Sci USA 99:10549–10554.

Varela M, Ramos C. 1996. Chondroectodermal dysplasia (Ellis-van Creveld syndrome): A case report. Eur J Orthodont 18: 313–318.

Yamauchi Y, Abe K, Mantani A, Hitoshi Y, Suzuki M, Osuzu F, Kuratani S, Yamamura K. 1999. A novel transgenic technique that allows specific marking of the neural crest cell lineage in mice. Dev Biol 212:191–203.

Zhang H, Takeda H, Tsuji T, Kamiya N, Kunieda T, Mochida Y, Mishina Y. 2017. Loss of function of Evc2 in dental mesenchyme leads to hypomorphic enamel. J Dent Res 96:414–422.

Zhang H, Takeda H, Tsuji T, Kamiya N, Rajderkar S, Louie KA, Collier C, Scott G, Ray M, Mochida Y, et al. 2015. Generation of Evc2/Limbin global and conditional KO mice and its roles during mineralized tissue formation. Genesis 53:612–626.